

ARTICLE OPEN

Protective molecular passivation of black phosphorus

Vlada Artel¹, Qiushi Guo², Hagai Cohen³, Raymond Gasper⁴, Ashwin Ramasubramaniam⁵, Fengnian Xia^{1,2} and Doron Naveh¹

Black phosphorus is a fascinating layered material, with extraordinary anisotropic mechanical, optical and electronic properties. However, the sensitivity of black phosphorus to oxygen and moisture poses significant challenges for technological applications of this unique material. Here, we report a viable solution that overcomes degradation of few-layer black phosphorus by passivating the surface with self-assembled monolayers of octadecyltrichlorosilane that provide long-term stability in ambient conditions. Importantly, we show that this treatment does not cause any undesired carrier doping of the bulk channel material, thanks to the emergent hierarchical interface structure. Our approach is compatible with conventional electronic materials processing technologies thus providing an immediate route toward practical applications in black phosphorus devices.

npj 2D Materials and Applications (2017)1:6; doi:10.1038/s41699-017-0004-8

INTRODUCTION

Black phosphorus (BP) is one of the most interesting layered materials, holding promise for emerging electronic and optoelectronic device technologies.^{1–4} The crystalline structure of BP displays in-plane anisotropy in addition to the out-of-plane anisotropy characteristic to layered materials.^{2, 5, 6} Therefore, BP supports anisotropic optical and transport responses that can enable unique device architectures.⁷ Its thickness-dependent direct bandgap varies in the range of 0.3–2.0 eV (from single-layer to bulk, respectively), making BP suitable to optoelectronics in a broad spectral range.^{8–10} With high room-temperature mobility, exceeding $1000 \text{ cm}^2 \text{ V}^{-1} \text{ s}^{-1}$ in thin films, BP is also a very promising material for electronics. However, BP is sensitive to oxygen and humidity¹¹ due to its threefold coordinated atoms. The surface electron lone pairs are reactive and can lead to structural degradation upon exposure to air, which in turn leads to significant deterioration in device performance in ambient conditions.^{12–14}

The unique and desirable optoelectronic properties of BP^{1, 3} have motivated much recent work to ameliorate its problematic air and moisture instability. Promising strategies to address this problem include the formation of a protective capping layer or a controlled stable native oxide¹⁵ at the surface. Capping of BP with two-dimensional layered materials such as graphene and hBN¹⁶ have provided stability for a period of 18 days. Alternatively, a 25 nm thick layer of alumina¹⁰ formed by atomic layer deposition was also found to be efficient, especially with the addition of a hydrophobic fluoropolymer layer that improved the stability over several weeks.¹⁷ More recently, organic functionalization of BP with layers of aryl diazonium has been shown to provide effective chemical passivation although this is accompanied by p-doping of the channel material.¹⁸ Here, we passivate BP with self-assembled monolayers (SAMs) of octadecyltrichlorosilane (OTS), thus gaining important advantages in terms of stability, oxidation resistance, and elimination of electronic devices degradation.

RESULTS AND DISCUSSION

SAMs are known for their effective surface passivation capabilities, particularly in semiconductor nanostructures.^{19, 20} OTS molecules, comprised of an eighteen carbon chain backbone, a trichlorosilane head group and a methyl (CH_3) functional group, can form smooth and uniform SAMs on oxidized substrates; these crystalline-like, close-packed SAMs²¹ can substantially reduce oxygen penetration toward the underlying reactive substrate. A scheme of our device structure is shown in Fig. 1a, where a thin native phosphorus oxide (BPO) layer bridges between OTS molecules and a BP crystal that forms the channel of a field-effect transistor (FET). The source and drain electrodes were defined by electron beam lithography on exfoliated BP flakes (8–10 nm thick) followed by metallization (Ti/Au). After liftoff, devices were cleaned with acetone and isopropanol and then immersed in hexane solution of OTS (see methods for details) for 1 h to obtain OTS coating on BP.

X-ray photoelectron spectroscopy (XPS) characterization, applied on bulk BP samples, clearly differentiates between the OTS-coated and uncoated BP, both exposed to air for the same period of time. Normalized P 2p core level spectra of coated (blue) and uncoated (red) BP are presented in Fig. 1b from which two pronounced differences are observed. First, in coated samples, the relative intensity of the broad peak around 134 eV, associated with BP oxide (BPO), is significantly smaller than in uncoated samples, indicating a thinner P-oxide layer as compared to bare BP. Because OTS coating of BP was performed in ambient conditions, a very thin layer of BPO still exists at the surface. Second, a pronounced spectral broadening of the low binding energy line (at ~ 130 eV) toward higher binding energies is imposed upon the OTS coating. A secondary, smaller broadening of the highly oxidized regime (at ~ 134 eV) toward lower binding energies is also seen. These spectral signatures of OTS-coated BP are further analyzed in detail and provide a possible mechanism for the surface reaction, as elaborated upon below.

¹Faculty of Engineering and Bar-Ilan Institute for Nanotechnology and Advanced Materials, Bar-Ilan University, Ramat-Gan 52900, Israel; ²Department of Electrical Engineering, Yale University, New Haven, CT 06511, USA; ³Department of Chemical Research Support, Weizmann Institute of Science, Rehovot 76100, Israel; ⁴Department of Chemical Engineering, University of Massachusetts Amherst, Amherst, MA 01003, USA and ⁵Department of Mechanical and Industrial Engineering, University of Massachusetts Amherst, Amherst, MA 01003, USA

Correspondence: Doron Naveh (doron.naveh@biu.ac.il)

Vlada Artel and Qiushi Guo contributed equally to this work.

Received: 5 November 2016 Revised: 14 December 2016 Accepted: 4 January 2017

Published online: 18 April 2017

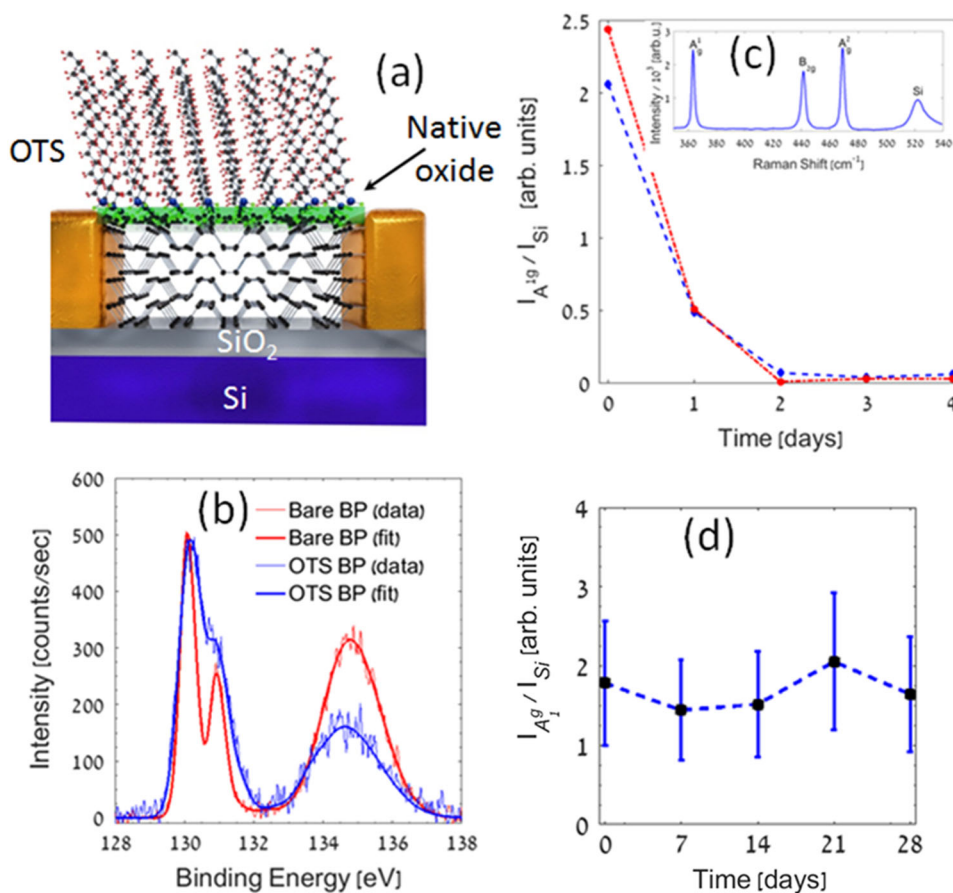


Fig. 1 **a** Structure of OTS-passivated BP in a FET device, showing a thin native oxide layer mediating the bonding of BP to OTS; **b** The P 2p XPS spectrum of bare (red) and OTS-coated (blue) BP together with their (red/blue) curve-fitting. Normalized time-resolved Raman spectra showing height ratios between the BP A_{1g} peak and the Si substrate peak at 520 cm⁻¹ of uncoated (c) and OTS-coated BP (d) samples. A full scanned spectrum is shown in the inset of c. Colors correspond to different samples in c

The efficiency of OTS passivation in preventing the typically rapid degradation of uncoated BP, is further confirmed by Raman spectroscopy, where the intensity of the A_{1g} peak of BP (normalized to the intensity of Si substrate peak at 520 cm⁻¹) provides a measure of sample's structural stability. In uncoated BP (Fig. 1c) a rapid decrease of the A_{1g} signal is observed, associated with the loss of long-range order,¹² due to oxidation and subsequent amorphization of the BP. In contrast, the spectra of OTS-coated samples (Fig. 1d) are stable to the level of fluctuations arising from variations between measurements. Complementary to the Raman analysis, optical microscopy of OTS-coated devices (Figs 2e–f) also shows no visible signs of degradation that are typical to BP.¹¹

The electronic properties probed by transport measurements of FET devices also show clear degradation of uncoated BP devices, with the current response decaying to negligible levels after 14 days (Fig. 2a; also see SI for additional data). Conversely, coated devices maintain their field-effect behavior over a period of 28 days, as shown in Fig. 2b. To ascertain whether the molecular layer dopes the BP, we measured the transport properties of the devices right before and immediately after coating, and found negligible variations in their transport characteristics. In particular, the negligible effect of OTS on threshold voltage (Fig. 2c and Fig. S4) precludes Fermi level shifts or charge transfer between BP and the molecular layer. Furthermore, the on/off current ratios (Fig. 2b and Fig. S3) prove that BP maintains its original electronic properties while stabilized with OTS. These results are significant and, notably, in contrast with other molecular layers such as aryl diazonium on BP,¹⁸ showing that BP preserves its original properties under the OTS coating. Figure 2d further demonstrates

that the transconductance (and hence, the hole mobility) is retained during the process of OTS self-assembly. Contrary to the decay of transport with time in bare BP (Fig. 2a) the stability of OTS-coated BP is remarkably persistent, suggesting that a robust corrosion-resistant molecular film is formed on the BP surface.

The success of OTS coatings in stabilizing BP and preserving its original electronic properties was studied in further detail by inspecting the SAM quality and its interaction with BP. Based on XPS (see SI for additional details) we conclude that a nearly vertically-aligned, ordered SAM is formed on the BPO (see Fig. 1a). We find a C:Si atomic ratio (extracted after elimination of background signals) of ~24, which is in excellent quantitative agreement with the value expected after correcting for the standard signal attenuation across the (CH₂)₁₇CH₃ backbone of the molecules. More precisely, the theoretical C:Si ratio for a perfect vertical orientation of the molecules is ≈26.4; hence, on average, slightly tilted molecules (~25° to the surface normal) better fit the experimentally extracted value.

Beneath the OTS layer, a thin (~2 nm) BPO layer is detected, consisting of low O:P stoichiometry, with a significant amount of partially oxidized P components, as shown in Fig. 3c. Importantly, the total signal of oxidized P-2p components (including those components of intermediate oxidation that appear in the coated sample only, as in Fig. 3c) normalized to the bulk BP signal, is roughly conserved in the coated samples with respect to uncoated ones. This fact suggests that limited reduction of pre-formed BPO takes place; a process involving removal of oxygen atoms, while the number of corresponding phosphorus atoms remains unaffected. In fact, the chemical reaction with OTS

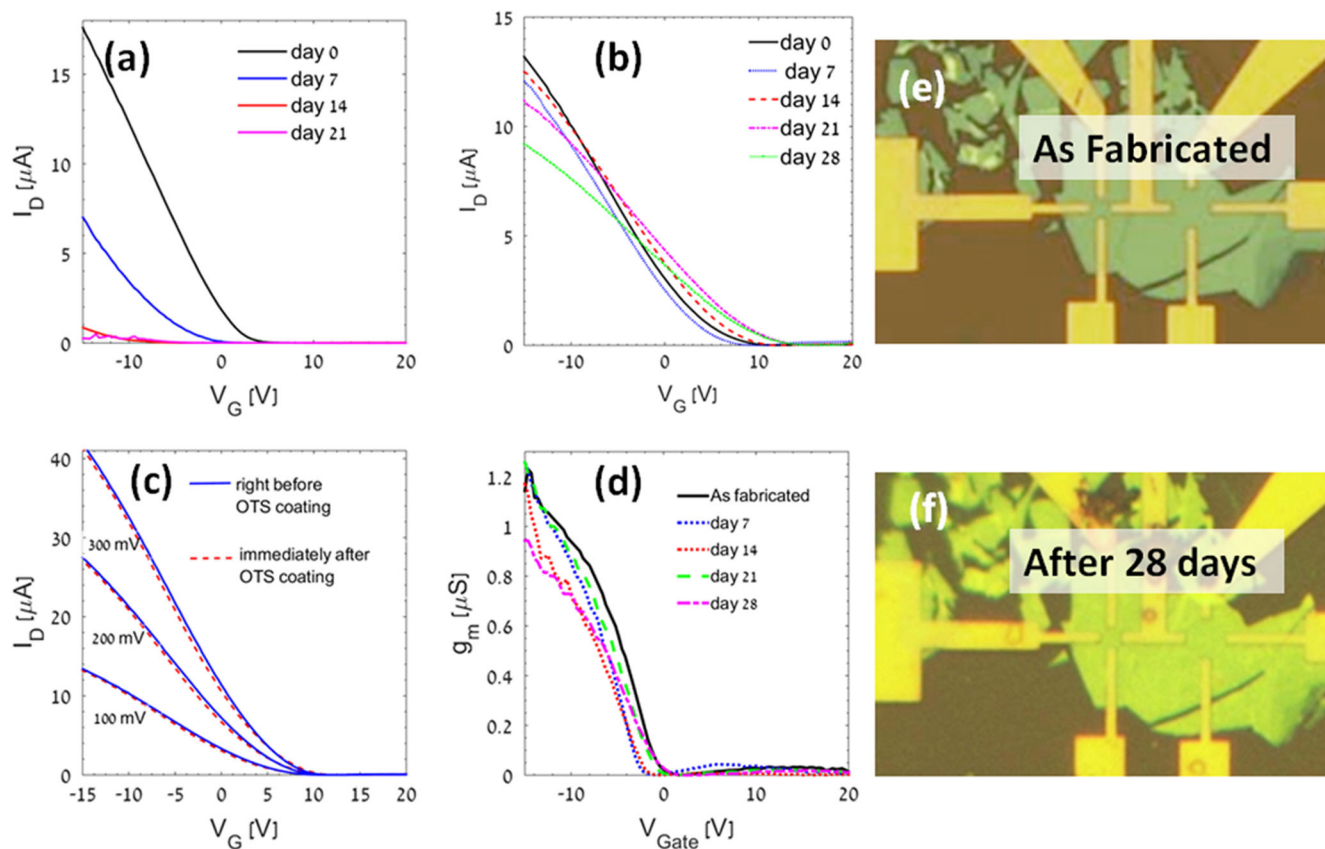


Fig. 2 Current transfer curves of uncoated (a) and OTS-coated (b) devices, sampled over a period of 28 days in room atmosphere. I–V curves of as-fabricated (uncoated, *solid lines*) and right after OTS-coating (*dotted curves*), showing negligible effect of the passivation treatment on device transfer curves (c), and device transconductance (d). Optical micrographs of the FET devices before OTS coating (e) and 28 days after OTS-coating (f)

involves the release of Cl atoms that are expected to cause mild reduction of the top BPO layer²¹ analogous to surface oxide reduction and corrosion of Al contacts in electronic devices.²² Remarkably, the amount of oxygen depleted from the BPO layer is comparable to the amount of oxygen required for the Si–Ox interface between BPO and OTS (see the SI for details). We, therefore, infer that the binding process of OTS is self-supported by the pre-existing BPO layer, which enables the success and robustness of our treatment.

Our proposed mechanistic interpretation is supported by multiple independent results. Firstly, based on our electrical measurements data we infer that no doping of the BP bulk takes place, which suggests that the bulk BP is indeed unaffected directly by the OTS. In other words, the thin oxide layer that is formed spontaneously, prior to OTS binding, seems to provide efficient protection against BP doping by any of the applied chemical agents. Also, no apparent traces of Cl atoms were observed on the BP surface, indicating that the hydrolysis reaction of OTS was complete. Secondly, controlled surface charging (CSC) data (Fig. S1) shows that BP remains highly conductive. The recorded line-shifts as the electron flood gun (eFG) was switched on and off were about 250 meV for the oxidized P, whereas the BP shifts were as small as 70 meV (see SI for details). As a reference, surrounding regimes of the adhesive tape shifted by ~600 meV under the very same conditions. This analysis suggests that the top BPO layer is slightly reduced during the exposure to OTS, such that the local stoichiometry changes from about $\text{PO}_{2.9}$ to about $\text{PO}_{1.5}$ on the average. Finally, computed binding energy shifts indicate (as discussed hereafter) a range of intermediate-oxidation states at the BPO/OTS interface that fit well our measured

intermediate P-signals in Fig. 3d, signals that are missing from the corresponding P 2p spectrum of uncoated BP.

Ab initio density functional theory (DFT) calculations were applied as an independent probe of the OTS binding to BP. The structural models considered consist of a unit cell of BPO in a low oxidation state,¹⁵ with a SAM of OTS in either a polymerized or a non-polymerized configuration (Fig. 3a, b). From DFT calculations, medium-binding-energy states (between 130–133 eV) were obtained, which is in line with the measured spectrum of the OTS-coated BP (Fig. 3c), where signals from partially oxidized states were resolved, as shown in Fig. 3d and further elaborated upon in the SI tables. The calculated chemical shifts (Tables S3 and S4) roughly fall into two categories: one set of states that are ~0.3–0.6 eV above the bulk P 2p level and a second set at ~1.8–1.9 eV above the lowest P 2p levels. While the actual structure of the surface oxide is most likely amorphous and hence, significantly more complex, the general agreement between core level energies for the surface-functionalized theoretical model and the XPS data supports the picture of chemical bonding, rather than mere physisorption, between the OTS molecules and the BPO.

To conclude, we have demonstrated a simple and effective strategy for efficient, long-term stabilization of BP surfaces against humidity and corrosion using OTS SAMs. This method can be applied to stabilize wafer-scale black phosphorus thin films in the future. In the process of attachment to BP, OTS partially reduces the pre-existing surface oxide, a process quantitatively evaluated by XPS. The stabilization of BP is independently confirmed by transport measurements, Raman spectroscopy and DFT calculations. We have shown that the native oxide layer of BP plays

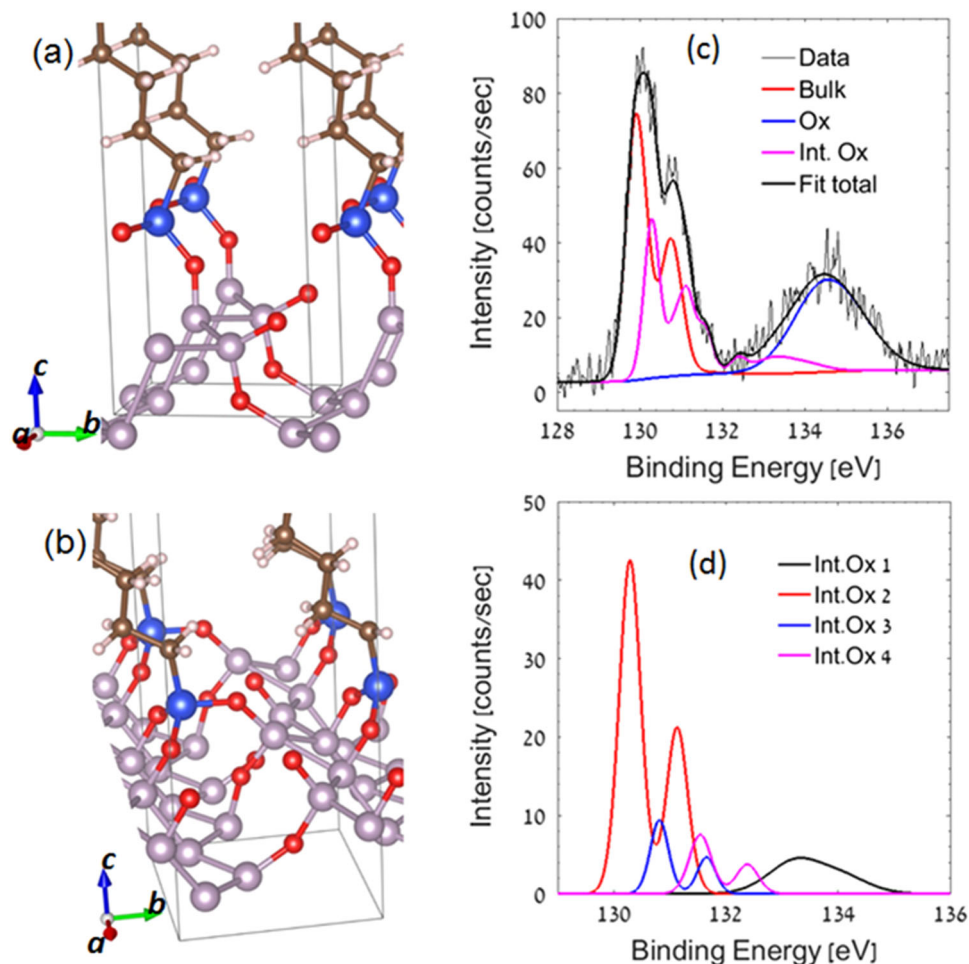


Fig. 3 The models used for calculations: A BPO monolayer passivated by OTS where **a** the OTS molecules polymerize (via Si-O-Si bonds) along a ridge, and **b** the OTS molecules bind only to surface oxygens without any polymerization. The BPO unit cell in **b** is doubled along the *a*-axis relative to that in **a**, to accommodate the OTS-binding configuration, resulting in $\frac{1}{2}$ -monolayer coverage. For clarity, only the part of OTS closest to the BPO layer is shown. (Atom colors: P-gray, O-red, Si-blue, C-brown, H-white). **c** The XPS P 2p line-shape analysis of coated BP, showing the intermediate oxidation states (pink) unique to the coated samples, together with the states common to all samples, bulk BP (red) and native oxide BPO (blue). **d** The four doublet components constructing the curve of intermediate P-states (the pink curve in panel **c**)

multiple critical roles in the surface functionalization process. Firstly, the BPO layer enables the binding of ordered, close-packed OTS layers by providing the oxygen for the hydrolysis process and presenting a flexible template for assembly. Secondly, the remaining thin oxide layer provides the necessary screening against undesired doping effects associated with inter-diffusion and charge transfer between BP and OTS. Finally, the oxide layer itself is stabilized by OTS and is part of the overall protective capping over the BP channel (see SI for more detail). Overall, this study provides an inexpensive, reliable, and scalable solution to the vexing stability problems of BP thus paving the way for future technological applications.

METHODS

OTS coating

OTS encapsulation was achieved by immersion of devices in 3 ml dry hexane solution containing 30 μ l of OTS for 1 h in a sealed tube to minimize air and moisture exposure. The samples were then washed in cold hexane and soaked for 10 min in hot hexane to remove OTS residues. Finally, samples were blow dried with nitrogen.

For coating bulk BP samples (HQ Graphene, 7803-51-2), the same anchoring procedure was performed, following immersion of BP for 1 min in 5% acetic acid solution (in acetone) and blow dried with nitrogen prior to soaking in OTS solution.

Raman spectroscopy

Raman spectra were collected on a Horiba Labram HR spectrometer with exciting laser line at 532 nm.

Device fabrication

BP flakes were mechanically exfoliated on a clean surface of 90 nm SiO₂/Si wafer. Electrodes were patterned by electron beam lithography and metallized with 3/50 nm Ti/Au.

XPS measurements

XPS measurements were carried out on a Kratos Axis Ultra DLD spectrometer, using monochromatic Al K α source at a relatively low power, in the range of 15–75 W. Samples were kept under inert atmosphere prior to their insertion into the vacuum, such that their exposure to air was limited to less than 1 min. The base pressure in the analysis chamber was kept below 10⁻⁹ Torr.

CSC^{23, 24} was used in order to differentiate between sample domains, as well as to eliminate signals originated from the underlying adhesive tape (see SI). The CSC data further provides information on the electrical properties of the resolved domains. Complementary measurements were performed on BP-flakes deposited on Ti and exposed to OTS at various conditions (not shown). Curve fitting was done using the Vision software, referring to control measurements on the bare adhesive tape and on samples dominated by polymerized OTS.

DFT calculations

Spin-polarized DFT calculations were performed using the Vienna ab initio Simulation Package.^{25, 26} The core and valence electrons were treated using the projector-augmented wave method.^{27, 28} The Perdew-Burke-Ernzerhof generalized-gradient approximation was used to describe electron exchange and correlation.²⁹ From convergence studies, a kinetic energy cutoff of 400 eV was chosen. Electronic convergence was accelerated with a Gaussian smearing of 0.05 eV for relaxation calculations; the Blöchl tetrahedron method³⁰ was used thereafter for single-point electronic structure calculations. Dipole corrections were applied along the vacuum direction of the supercell (normal to BPO layer). Core-level shifts were calculated in the initial-state approximation.

CHANGE HISTORY

A correction to this article has been published and is linked from the HTML version of this article.

ACKNOWLEDGEMENTS

D.N. acknowledges support from the Israel Science Foundation (ISF grant No. 2174/15 and ISF grant No. 1055/15). R.G. and A.R. acknowledge computational support from the Massachusetts Green High-Performance Computing Center. F.X. thanks the National Science Foundation (EFMA-1542815) and Air Force Office of Scientific Research (FA9550-14-1-0277) for the financial support.

AUTHOR CONTRIBUTIONS

V.A. and Q.G. fabricated the devices and performed Raman and electrical measurements. H.C. and V.A. performed XPS measurements and analysis. R.G. and A.R. performed theoretical calculations and analysis. D.N. and F.X. conceived the idea, designed the experiments and analyzed the data. All authors discussed the results and commented on the manuscript.

COMPETING INTERESTS

The authors declare no competing interests.

REFERENCES

1. Li, L. *et al.* Black phosphorus field-effect transistors. *Nat. Nanotechnol.* **9**, 372–377 (2014).
2. Ling, X., Wang, H., Huang, S., Xia, F. & Dresselhaus, M. S. The renaissance of black phosphorus. *Proc. Natl Acad. Sci.* **112**, 4523–4530 (2015).
3. Xia, F., Wang, H. & Jia, Y. Rediscovering black phosphorus as an anisotropic layered material for optoelectronics and electronics. *Nat. Commun.* **5**, (2014).
4. Liu, H. *et al.* Phosphorene: an unexplored 2D semiconductor with a high hole mobility. *ACS Nano* **8**, 4033–4041, doi:10.1021/nn501226z (2014).
5. Xia, F., Wang, H., Xiao, D., Dubey, M. & Ramasubramanian, A. Two-dimensional material nanophotonics. *Nat. Photon.* **8**, 899–907 (2014).
6. Wang, X. *et al.* Highly anisotropic and robust excitons in monolayer black phosphorus. *Nat. Nanotechnol.* **10**, (2015).
7. Tian, H. *et al.* Anisotropic black phosphorus synaptic device for neuromorphic applications. *Adv. Mater.* **28**, 4991–4997 (2016).
8. Guo, Q. *et al.* Black phosphorus mid-infrared photodetectors with high gain. *Nano. Lett.* **16**, 4648–4655 (2016).
9. Engel, M., Steiner, M. & Avouris, P. Black phosphorus photodetector for multi-spectral, high-resolution imaging. *Nano. Lett.* **14**, 6414–6417 (2014).

10. Buscema, M. *et al.* Fast and broadband photoresponse of few-layer black phosphorus field-effect transistors. *Nano. Lett.* **14**, 3347–3352 (2014).
11. Joshua, O. I., Gary, A. S., Herre, S. JvdZ. & Andres, C.-G. Environmental instability of few-layer black phosphorus. *2D Materials* **2**, 011002 (2015).
12. Wood, J. D. *et al.* Effective passivation of exfoliated black phosphorus transistors against ambient degradation. *Nano. Lett.* **14**, 6964–6970 (2014).
13. Island, J. O., Steele, G. A., van der Zant, H. S. & Castellanos-Gomez, A. Environmental instability of few-layer black phosphorus. *2D Materials* **2**, 011002 (2015).
14. Ziletti, A., Carvalho, A., Campbell, D. K., Coker, D. F. & Castro Neto, A. H. Oxygen defects in phosphorene. *Phys. Rev. Lett.* **114**, 046801 (2015).
15. Edmonds, M. *et al.* Creating a stable oxide at the surface of black phosphorus. *ACS Appl. Mater. Interfaces* **7**, 14557–14562 (2015).
16. Doganov, R. A. *et al.* Transport properties of pristine few-layer black phosphorus by van der Waals passivation in an inert atmosphere. *Nat. Commun.* **6**, (2015).
17. Kim, J. -S. *et al.* Toward air-stable multilayer phosphorene thin-films and transistors. *Sci. Rep.* **5**, (2015).
18. Ryder, C. R. *et al.* Covalent functionalization and passivation of exfoliated black phosphorus via aryl diazonium chemistry. *Nat. Chem.* **8**, 597–602 (2016).
19. Schwartzman, M., Sidorov, V., Ritter, D. & Paz, Y. Surface passivation of (100) InP by organic thiols and polyimide as characterized by steady-state photoluminescence. *Semicond. Sci. Technol.* **16**, L68 (2001).
20. Mastronardi, M. L. *et al.* Size-dependent absolute quantum yields for size-separated colloidal-stable silicon nanocrystals. *Nano. Lett.* **12**, 337–342, doi:10.1021/nl2036194 (2012).
21. Ulman, A. Formation and structure of self-assembled monolayers. *Chem. Rev.* **96**, 1533–1554 (1996).
22. Nihonyanagi, S., Eftekhari-Bafrooei, A., Hines, J. & Borguet, E. Self-assembled monolayer compatible with metal surface acoustic wave devices on lithium niobate. *Langmuir* **24**, 5161–5165 (2008).
23. Doron-Mor, I. *et al.* Controlled surface charging as a depth-profiling probe for mesoscopic layers. *Nature* **406**, 382–385 (2000).
24. Shabtai, K., Rubinstein, I., Cohen, S. R. & Cohen, H. High resolution lateral differentiation using a macroscopic probe: XPS of organic monolayers on composite Au-SiO₂ surfaces. *J. Am. Chem. Soc.* **122**, 4959–4962 (2000).
25. Kresse, G. & Furthmüller, J. Efficient iterative schemes for Ab initio total-energy calculations using a plane-wave basis set. *Phys. Rev. B* **54**, 11169–11186 (1996).
26. Kresse, G. & Hafner, J. Ab initio molecular dynamics for liquid metals. *Phys. Rev. B* **47**, 558 (1993).
27. Kresse, G. & Joubert, D. From ultrasoft pseudopotentials to the projector augmented-wave method. *Phys. Rev. B* **59**, 1758–1775 (1999).
28. Blöchl, P. E. Projector augmented-wave method. *Phys. Rev. B* **50**, 17953 (1994).
29. Perdew, J. P., Burke, K. & Ernzerhof, M. Generalized gradient approximation made simple. *Phys. Rev. Lett.* **77**, 3865–3868 (1996).
30. Blöchl, P. E., Jespen, O. & Andersen, O. K. Improved tetrahedron method for brillouin-zone integrations. *Phys. Rev. B* **49**, 16223 (1994).



This work is licensed under a Creative Commons Attribution 4.0 International License. The images or other third party material in this article are included in the article's Creative Commons license, unless indicated otherwise in the credit line; if the material is not included under the Creative Commons license, users will need to obtain permission from the license holder to reproduce the material. To view a copy of this license, visit <http://creativecommons.org/licenses/by/4.0/>

© The Author(s) 2017

Supplementary Information accompanies the paper on the *npj 2D Materials and Applications* website (doi:10.1038/s41699-017-0004-8).